JACS Au
AN OPEN ACCESS JOURNAL OF THE AMERICAN CHEMICAL SOCIETY

pubs.acs.org/jacsau
Article

Different DNA Binding and Damage Mode between Anticancer Antibiotics Trioxacarcin A and LL-D49194α1

Ruo-Qin Gao, Xiao-Dong Hu, Qiang Zhou, Xian-Feng Hou, Chunyang Cao,* and Gong-Li Tang*

Cite This: JACS Au 2024, 4, 3641−3648
Read Online

ACCESS | Metrics & More | Article Recommendations | Supporting Information

ABSTRACT: Trioxacarcin A (TXN) is a highly potent cytotoxic antibiotic with remarkable structural complexity. The crystal structure of TXN bound to double-stranded DNA (dsDNA) suggested that the TXN interaction might depend on positions of two sugar subunits on the minor and major grooves of dsDNA. LL-D49194α1 (LLD) is a TXN analogue bearing the same polycyclic polyketide scaffold with a distinct glycosylation pattern. Although LLD was in a phase I clinical trial, how LLD binds to dsDNA remains unclear. Here, we solved the solution structures at high resolutions of palindromic 2″-fluorine-labeled guanine-containing duplex $d(A_1A_2C_3C_4G^FG^FT_7T_8)_2$ and of its stable LLD and TXN covalently bound complexes. Combined with biochemical assays, we found that TXN-alkylated dsDNA would tend to keep DNA helix conformation, while LLD-alkylated dsDNA lost its stability more than TXN-alkylated dsDNA, leading to dsDNA denaturation. Thus, despite lower cytotoxicity in vitro, the differences of sugar substitutions in LLD caused greater DNA damage than TXN, thereby bringing about a completely new biological effect.

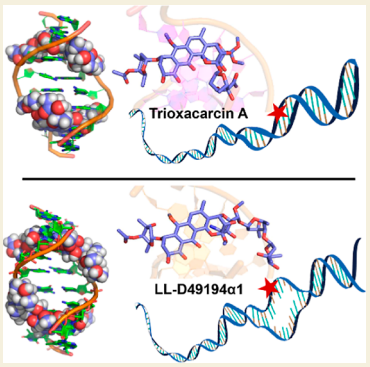

KEYWORDS: *trioxacarcin A, LL-D49194α1, NMR structure, DNA binding, DNA alkylation, DNA damage, anticancer polyketide*

INTRODUCTION

Anthracyclines are clinically useful anticancer agents with structural diversity; they often display DNA intercalation property for the planar aromatic ring system with glycosyl modifications. For example, the anticancer drugs daunorubicin and doxorubicin intercalate with DNA noncovalently,[1] while hedamycin, trioxacarcin A (TXN), as well as its analogues LL-D49194α1 (LLD) and LL-D49194β2 (Figure 1A,B) all contain spiro-epoxides, which can intercalate and alkylate DNA.[2−5] As an atypical member of anthracyclines, LLD was first isolated from *Streptomyces vinaceusdrappus* NRRL 15735 and displayed a range of biological effects especially antitumor activity.[6] Due to its antitumor activity and low toxicity profile in experimental animal, LLD was subjected to clinical phase I trials in the early 1990s in 15 patients with histologically confirmed metastatic cancer,[7] although it was suspended due to unexpected cardiotoxicity.

LLD and TXN shared a common highly oxygenated, polycyclic rigid skeleton but differed in glycosylation and methylation modifications at C-13 −OH and C-16 −OH groups (Figure 1A,B). Previous studies implied that LLD shared the same reactive site with TXN by which it alkylates G of duplex DNA (Figure 1C).[5] The spiro-epoxide functional group of TXN can efficiently and irreversibly alkylate guanine base (G) of duplex or G-quadruplex DNA via nucleophilic addition reaction,[3,8] forming a covalent bond between C-17 of the epoxide and N-7 of alkylated G (Figure 1C). A reported crystal structure of TXN-bound $d(A_1A_2C_3C_4G_5G_6T_7T_8)_2$ (pdb code 3C2J) suggested that TXN insertion into the DNA helix was probably stabilized by the location of both bulky sugar rings in the minor and major grooves, which induced flipping-out of a single, nonterminal nucleobase thymine away from a DNA duplex (Figure 1D).[9]

In the past 10 years, many analogues of TXN and LLD were chemically or biologically synthesized,[10−18] and biological activity investigations further confirmed the importance of both glycosyl substituents. Discovered nearly 10 years later than TXN with different glycosyl substituents, LLD showed obviously weaker antitumor activity by about 10 times during cytotoxicity assay in vitro.[11,17,19] However, LLD, which was discovered later, successfully entered clinical trials earlier than TXN for better preclinical profile in animal experiments in vivo.[6,20] This inspired us to explore the underlying mechanism stemming from the distinct glycosyl substitutions.

Since 2014, we have performed continuously biosynthetic studies of TXN and LLD,[12,14,17,18,21−23] which provided us enough compounds to study the DNA binding and damage analysis. To explore how LLD interacted with double-stranded DNA (dsDNA) under near-physiological conditions, we decided to use TXN as a reference to compare the details of their reaction with DNA by nuclear magnetic resonance (NMR)

Received: July 8, 2024
Revised: August 28, 2024
Accepted: August 28, 2024
Published: September 10, 2024

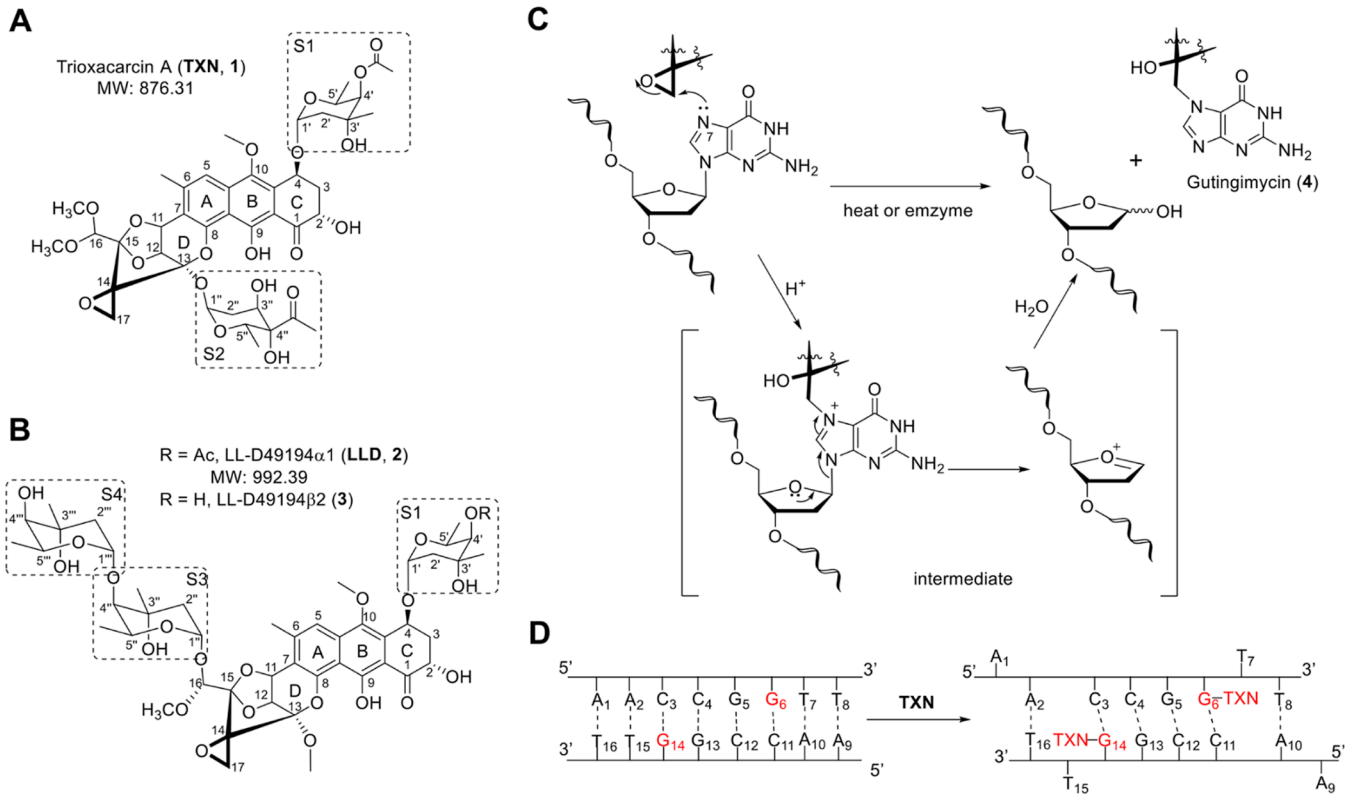

Figure 1. Trioxacarcin family of natural products as DNA alkylating agents. (A,B) Structures of trioxacarcin A (TXN), LL-D49194α1 (LLD), and LL-D49194β2; (C) DNA alkylation reaction by TXN or LLD; (D) model of TXN covalently interacting with dsDNA based on the structure 3C2J. The alkylated sites are in red.

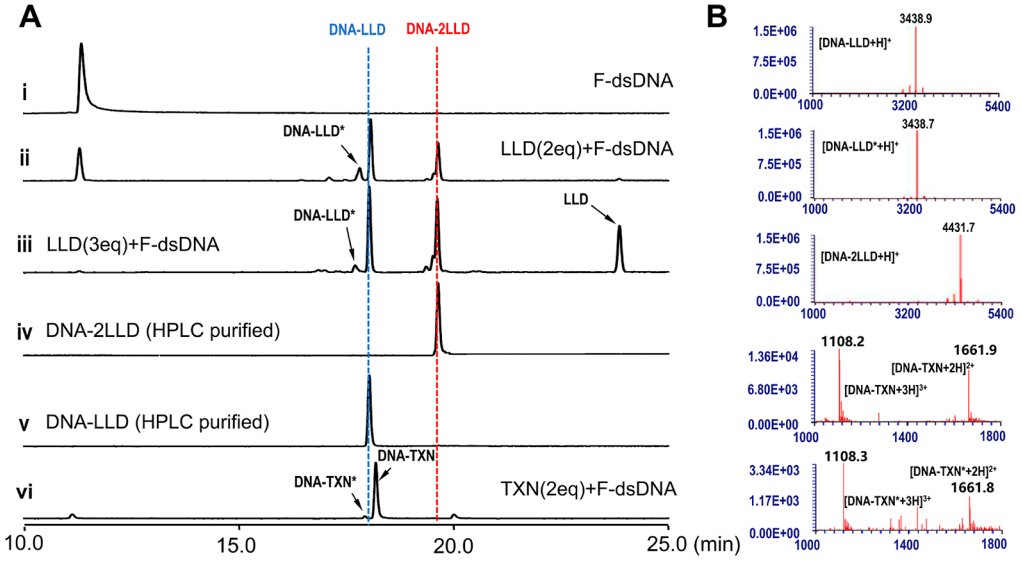

Figure 2. Production profiles of TXN or LLD alkylation on F-dsDNA. (A) Reaction systems detected by HPLC. (i) Standard sample of F-dsDNA, (ii) reactions between F-dsDNA and double equivalent LLD, (iii) F-dsDNA reacted with excess LLD (3 equiv), (iv and v) each LLD alkylation product purified by HPLC, and (vi) F-dsDNA reacted with double equivalent TXN. (B) Mass spectra with m/z of each alkylation product observed in the reactions.

technologies combined with biochemical assays. During this study, we found that TXN and LLD led to different kinds of DNA damage based on the same chemical reaction. We also provided the structural basis for the biological activities of these molecules and indicated the roles played by their various substituents, providing a theoretical basis for future structural modifications of this family of compounds.

RESULTS

DNA Alkylation Products by LLD Were Different from Those by TXN

To begin with, the dsDNA with a sequence d-$(A_1A_2C_3C_4G_5G_6T_7T_8)_2$ (which was used in crystal structure 3C2J) was selected. Given the fact that G usually undergoes

https://doi.org/10.1021/jacsau.4c00611
JACS Au 2024, 4, 3641−3648

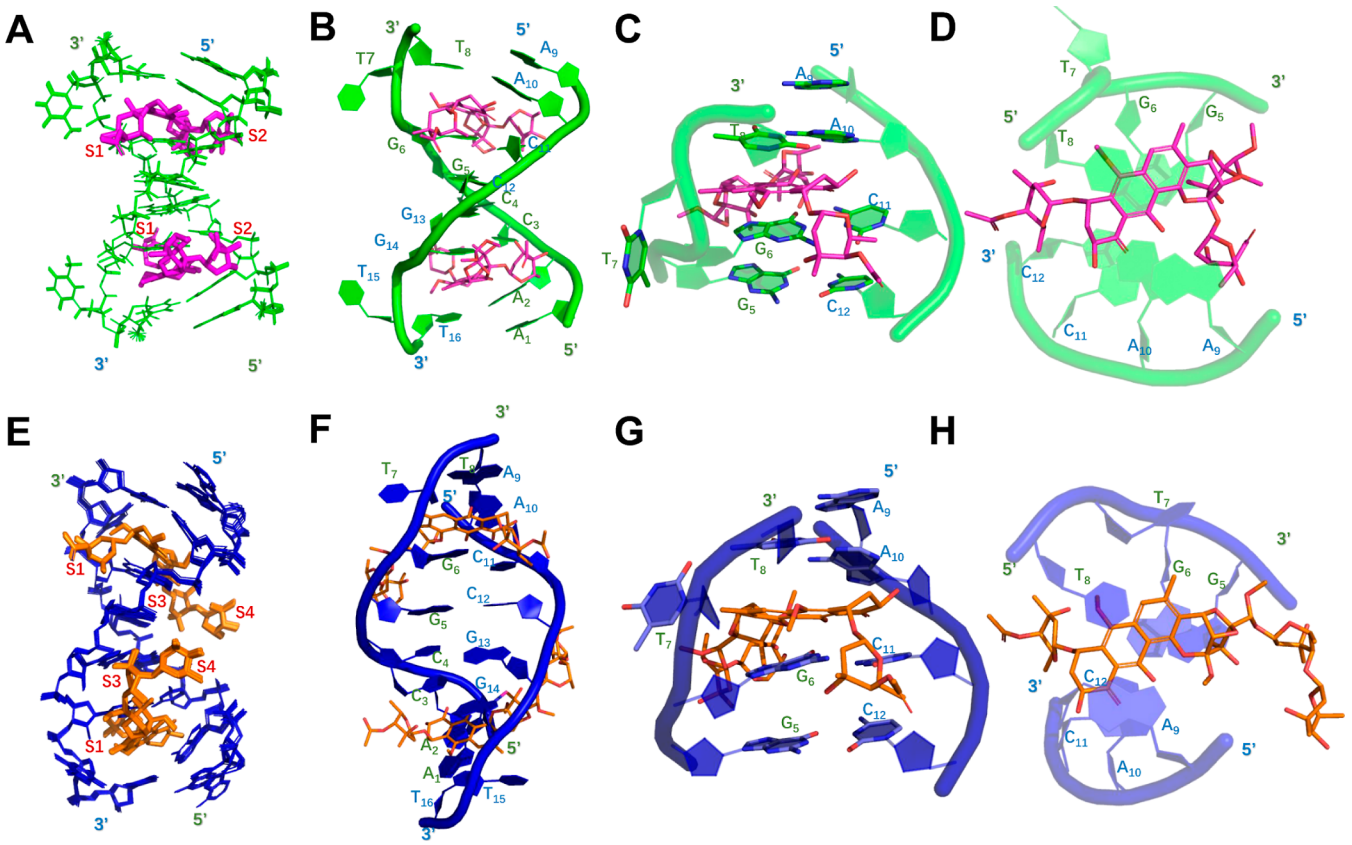

Figure 3. Structural comparison of TXN and LLD covalently bound dsDNA complexes. (A,E) Ensemble of 20 overlapped structures with the lowest energy of $(DNA-TXN)_2$ (A) and $(DNA-LLD)_2$ (E) in solution. (B,F) One representative structure displayed in stick and in cartoon mode of $(DNA-TXN)_2$ (B) and $(DNA-LLD)_2$ (F). (C,G) Drug is covalently bound to G_6 and intercalated on its 3′-side between base pair G_6-C_{11} and $A_{10}-T_8$, and T_7 was flipped-out. (C, D, G, and H) Lateral and vertical view of $(DNA-TXN)_2$ (D,E) and $(DNA-LLD)_2$ (G,H) showed drug backbone planes parallel to base pairs. TXN and LLD are shown in pink and orange, respectively.

dealkylation after it reacts with alkylating reagents, d-$(A_1A_2C_3C_4G^FG^FT_7T_8)_2$ (i.e., F-dsDNA for simplicity hereinafter), in which the 2″ positions of the guanine sugar rings were fluorinated, was used to avoid cleavage of the glycosyl bond between sugar and the alkylated G.[24] The fluorine-labeled single-stranded oligo $d(A_1A_2C_3C_4G^FG^FT_7T_8)$ (i.e., F-ssDNA, MW: 2445.54) was commercially synthesized, purified, and dialyzed, and then F-dsDNA was made by annealing (10 mM phosphate, 20 mM NaCl, pH 7.2). Incubation of this F-dsDNA with LLD was progressed at 277 K and tested by high-performance liquid chromatography−ultraviolet (HPLC−UV). For LLD, three alkylation products were observed on a denatured HPLC system, including two kinds of monoalkylated forms (i.e., DNA-LLD and DNA-LLD*, Figure 2A, lines ii, iii, and v) and one sort of dialkylated oligonucleotide single chains (i.e., DNA-2LLD, Figure 2A, lines ii−iv). Moreover, the ratio of minor monoalkylated product DNA-LLD* did not increase with the addition of more LLD and an excessive amount of LLD will not further alkylate DNA-LLD to generate DNA-2LLD (Figure 2A, lines ii and iii). In contrast, TXN alkylation mainly generated a single product with one alkylation site in each single chain (i.e., DNA−TXN, Figure 2A, line vi), although a small peak beside DNA−TXN with the same molecular mass was observed (i.e., DNA−TXN*, line vi). Generation of alkylated DNA oligos was consistent with a characteristic absorption at near 400 nm of TXN/LLD in UV−vis spectra (Figure S1) and confirmed by mass spectroscopy (Figure 2B). The single alkylation site on F-dsDNA by LLD or TXN was F-labeled G_6 (also G_{14} in complementary strand, similarly hereinafter), in line with the chemical shift perturbation of the protons in F-dsDNA after interaction with TXN and LLD (Figure S2). The second alkylation site on F-dsDNA by LLD was F-labeled G_5 (G_{13}).

Solution Structure of LLD-Alkylated dsDNA Presented Unstable dsDNA Conformation

For free F-dsDNA, the imino proton signals G_5 (G_{13}), G_6 (G_{14}), and T_7 (T_{15}) were observed at the region 12−14.5 ppm in its one-dimensional [i.e., one-dimensional (1D)] ^{1}H NMR spectrum (Figure S3A), indicating that the F-labeled dsDNA was in the classical B-form. Subsequently, we enriched alkylated single-stranded oligos DNA−TXN, DNA−LLD, and DNA−2LLD for NMR analysis. The signals belonging to the imino protons were observed in the 1D ^{1}H NMR spectra (Figures S3B,C) acquired on the annealed $(DNA-TXN)_2$ and $(DNA-LLD)_2$ samples, suggesting that G alkylation by either TXN or LLD maintained partial helix structures of dsDNA. In contrast, the imino proton signals disappeared in the 1D ^{1}H NMR spectrum of the annealed DNA−2LLD sample (Figure S3D), implying that DNA−2LLD was a free single chain. Therefore, only free F-dsDNA and covalent $(DNA-TXN)_2$ and $(DNA-LLD)_2$ complexes were employed to acquire a series of two-dimensional NMR spectra for structural studies. After signal assignment (Tables S1−S5 and Figure S4), we successfully obtained a large number of intrabase NOEs in F-dsDNA and intra-TXN or LLD NOEs, especially intermolecular NOEs

https://doi.org/10.1021/jacsau.4c00611
JACS Au 2024, 4, 3641−3648

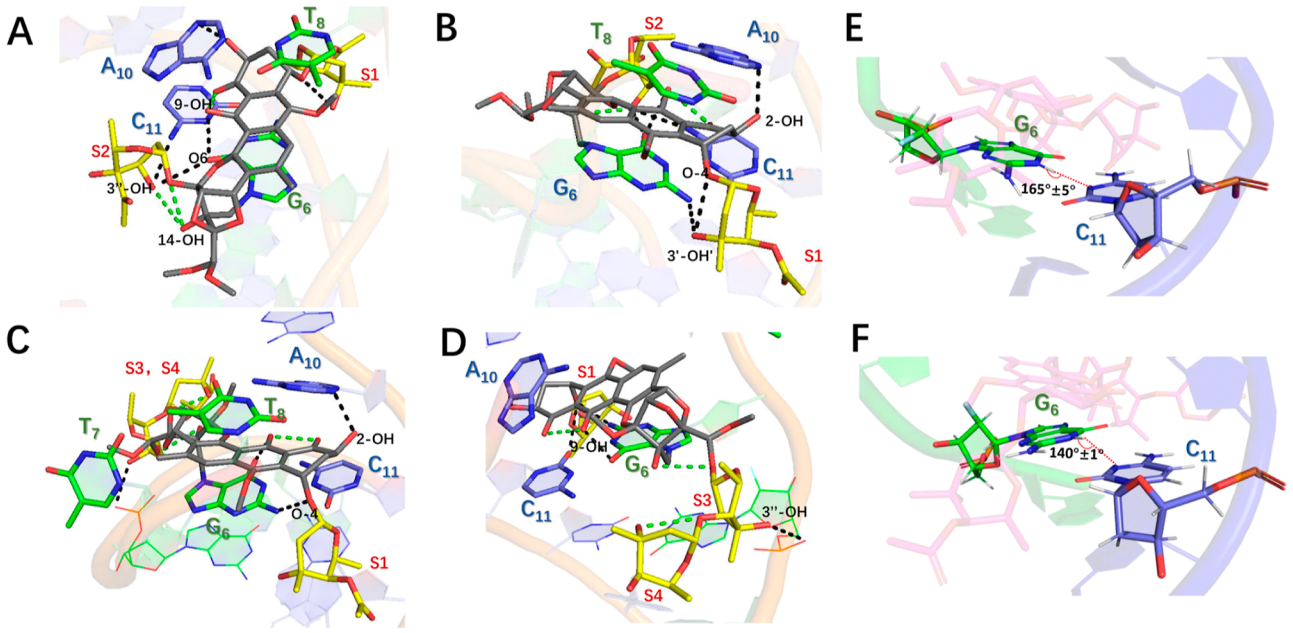

Figure 4. Structural analysis on covalent $(DNA-TXN)_2$ and $(DNA-LLD)_2$ complexes. (A,B) Hydrogen bond net formed in the $(DNA-TXN)_2$ complex structure. (C,D) Hydrogen bond net observed in the $(DNA-LLD)_2$ complex structure. (E,F) Effects on G_6-C_{11} base pair planes by TXN or LLD alkylation in $(DNA-TXN)_2$ (E) and $(DNA-LLD)_2$ (F) complexes. In (A–D), all residues are in stick mode, TXN or LLD in black, sugar S1, S2, S3, and S4 in yellow. Intra-TXN intra-LLD hydrogen bonds are in green, and the hydrogen bonds between TXN or LLD and bases are in black. In (E,F), TXN or LLD is in pink stick, and the DNA bases are in green (G_6) and blue (C_{11}) stick.

between TXN or LLD and bases in F-dsDNA (Figure S5 and Tables S6) for further structural determination.

To account for how LLD alkylated dsDNA, the solution structures of free F-dsDNA and two covalent complexes $(DNA-TXN)_2$ and $(DNA-LLD)_2$ were calculated (356, 748, and 736 NOE-derived distance constraints; 94, 112, and 96 dihedral constraints; 60, 66, and 66 hydrogen-bonds; Table S7). F-dsDNA (pdb code: 8Y1I) was still in the B-form (Figure S6), and the overall NMR structure of $(DNA-TXN)_2$ (pdb code: 8XIC) in solution (Figure 3A) was roughly identical to the reported crystal structure (3C2J), with an rmsd value of 2.11 Å (Figure S7A). TXN alkylated bases G_6 (G_{14}), inserted into the DNA B-helix (Figure 3B), and occupied the position of base T_7 (T_{15}), resulting in their flipping out away from the dsDNA helix, and new T_8-A_{10} and $T_{16}-A_2$ base pairs were formed. The planar aromatic rings A and B and partial aliphatic ring C of TXN were almost parallel to $G_{14}-C_3$ (G_6-C_{11}) and A_2-T_{16} ($A_{10}-T_8$) base pairs by $\pi-\pi$ stacking (Figure 3C,D), supported by the observed NOEs (Figures S8 and S9). The C-4 linked sugar S1 was positioned in the minor groove of dsDNA, while the C-13 connected sugar S2 was located in the major groove (Figure 3A), evidenced by some NOE correlations (Figure S10). The base A_1 (A_9) was parallel to the newly formed base pair A_2-T_{16} ($A_{10}-T_8$) (Figure 3B). The first intermolecular hydrogen bond net was observed between the 3″−OH group in sugar S2 and the base C_3 (C_{11}) $-NH_2$ group, between the carbonyl O-6 atom of G_6 (G_{14}) and 9-OH of TXN, and between the 3″−OH group in sugar S2 and the carbonyl O-6 atom of G_6 (G_{14}) (Figure 4A). The second hydrogen bond net was found among the O-4 atom, 3′−OH in sugar S1 of TXN, and the base G_6 (G_{14}) $-NH_2$ group and between the N-3 atom of A_2 (A_{10}) and 2-OH of TXN (Figure 4B). All these H-bonds fixed the conformation of covalently bound TXN in the complex.

The overall structure of the LLD (pdb code: 8XC7) covalently bound F-dsDNA complex has a degree of similarity to the TXN-bound DNA complex, with an rmsd value of 2.06 Å (Figure S7B). The alkylation site and the mode of binding at the minor groove of dsDNA are similar between them. LLD covalently bound to the 3′ terminal G_6 (G_{14}), which led to base T_7 (T_{15}) flipping out away from the dsDNA helix (Figure 3E,F) (NOE evidence in Figure S12), and LLD took their positions up completely. The aromatic rings A and B and partial aliphatic ring C were parallel to the base pairs G_6-C_{11} ($G_{14}-C_3$) and A_2-T_{16} ($A_{10}-T_8$) by $\pi-\pi$ stacking (Figure 3G,H) (NOE evidence in Figure S13). The C-4 linked sugar ring S1 of LLD is also located in the minor groove (Figure 3E), similar to that observed in the $(DNA-TXN)_2$ complex (Figure 3A) with almost identical interactions (Figure S15). However, it was different from TXN where the intermolecular hydrogen bonds were observed between the amino group of alkylated G_6 (G_{14}) and the O-4 atom of ring C (Figure 4C). Great differences were found at the major groove of dsDNA. The large C-16-substituted tandem sugar rings S3 and S4 of LLD were positioned in the major groove of F-dsDNA (Figure 3E) (NOEs in Figure S15). Only four weak intermolecular NOEs between the sugar rings S3 and S4 and bases were observed (Table S6), which meant the long tandem linked sugars interacted weakly with dsDNA. Moreover, only one intermolecular hydrogen bond between 3′′−OH in LLD sugar S3 and one of backbone oxygen atoms (O1P) of base G_5 (G_{13}) was observed with a distance of 2.9 Å (Figure 4D). The 9-OH group of LLD formed a hydrogen bond with a carbonyl O-6 atom of G_6 (G_{14}), similar to TXN. However, the −OH group at the C-14 position, generated from the alkylation reaction of the spiro-epoxide ring with the N-7 atom of base G_6 (G_{14}), did not show any hydrogen bond interactions with −OH groups in sugar rings S3 and S4; therefore, the long glycosyl substituents in LLD were flexible to interact with the phosphate backbone.

Interestingly, the imino atoms N1 and H1 of base G_6 (G_{14}) and the O6 atom of base C_{11} (C_3) in the hydrogen bond formed an averaged angle 140 ± 1° in $(DNA-LLD)_2$ complex, smaller

https://doi.org/10.1021/jacsau.4c00611
JACS Au 2024, 4, 3641−3648

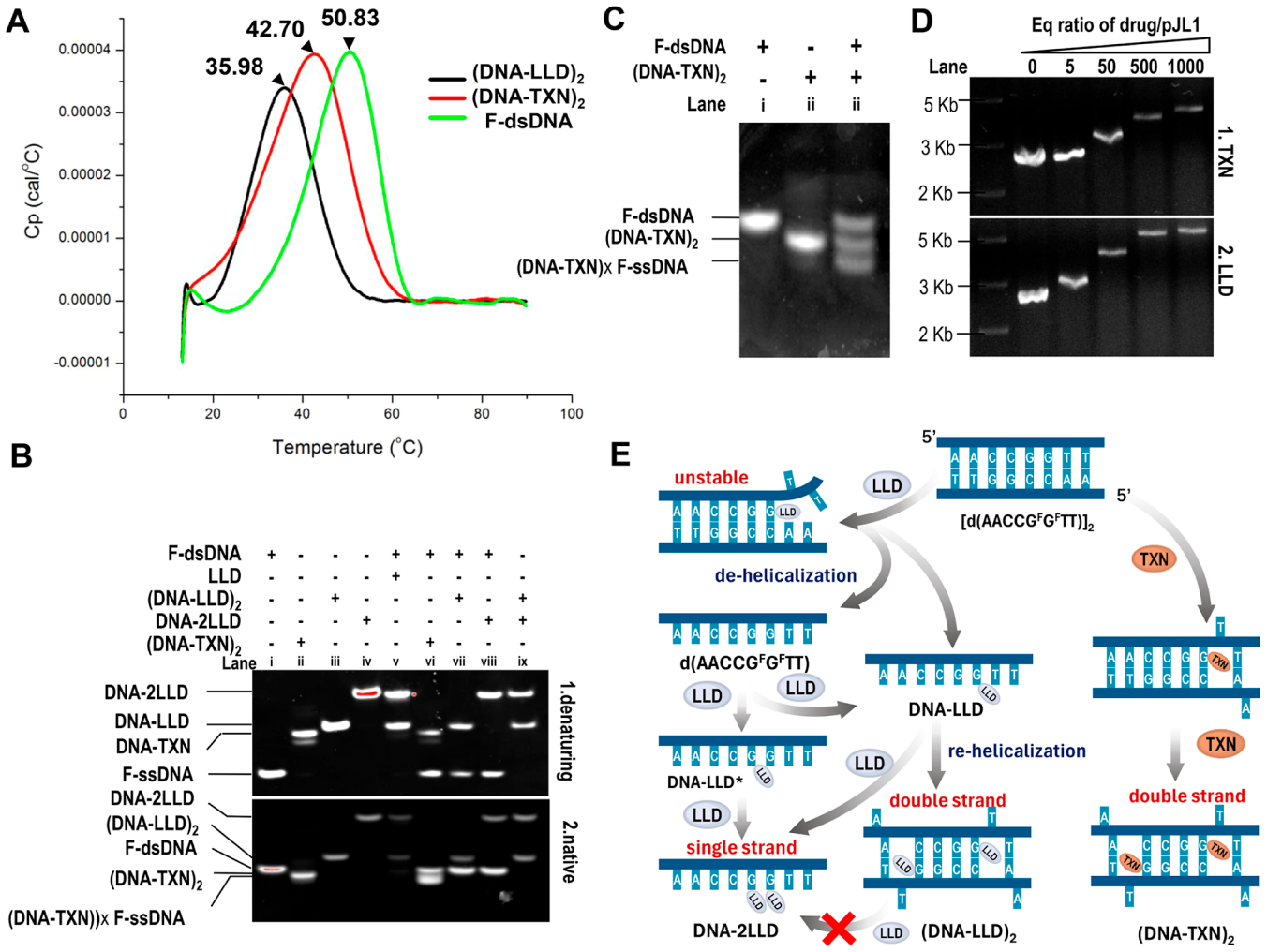

Figure 5. Effects on the structure and stability of dsDNA due to TXN and LLD alkylation. (A) T_m values of free F-dsDNA, $(DNA–TXN)_2$, and $(DNA–LLD)_2$; (B) single- or double-stranded oligos detected by denaturing (up) and native (down) PAGE gels (TBE gels, 20%). Lanes (v), reaction system of F-dsDNA and LLD (1:3); (vi–ix) results of hybridization experiments. (C) Hybridization results of $(TXN–DNA)_2$ with F-dsDNA tested by native PAGE (TBE gels, 22%) with better resolution. (D) Alkylation reaction of linearized plasmid pJL1 with TXN (up) and LLD (down), respectively, detected by Agarose gel. (E) Proposed alkylation mode of TXN and LLD on dsDNA.

than that (165 ± 5°) in the $(DNA–TXN)_2$ complex (Figure 4E,F), suggesting that the LLD-alkylated base G_6 (G_{14}) was not completely in plane with base C_{11} (C_3) in the covalent $(DNA–LLD)_2$ complex. This observation implied that the large, flexible, and steric sugar rings S3 and S4 weakened the $\pi–\pi$ stacking effects between LLD aromatic rings A and B and base pairs $G_6–C_{11}$ ($G_{14}–C_3$) and $A_2–T_{16}$ ($A_{10}–T_8$) and caused instability of dsDNA. This conclusion was further supported by T_m values [measured by differential scanning calorimetry (DSC) assay] of free F-dsDNA (50.83 °C), $(DNA–TXN)_2$ (42.70 °C), and $(DNA–LLD)_2$ (35.98 °C) (Figure 5A). In addition, the largest enthalpy value (ΔH_M) generally meant the strongest $\pi–\pi$ stacking between residues in dsDNA.[25] The order of the ΔH_M values of F-dsDNA, $(DNA–TXN)_2$, and $(DNA–LLD)_2$ was $(DNA–TXN)_2$ > F-dsDNA > $(DNA–LLD)_2$ (Table S8), implying that stacking interactions among base pairs and TXN in $(DNA–TXN)_2$ were much stronger than those in the $(DNA–LLD)_2$ complex, so the conformation of $(DNA–TXN)_2$ was more stable and compact than that of $(DNA–LLD)_2$.

LLD-Alkylated DNA Double Helix Was More Unstable Than TXN-Alkylated dsDNA

To testify the different effects on the structure and stability of dsDNA by TXN or LLD alkylation, native and denaturing PAGE gels were performed, where DNA dyed by EB would show red fluorescence, while the backbones of TXN or LLD were green at 300 nm. In denaturing gel, the migration rate of gel electrophoresis is negatively correlated with the molecular weight that alkylated DNA migrated more slowly than free dsDNA (lanes i–ix, upper Figures 5B and S16; the small bands in lanes ii and vi might be minimal DNA–TXN*). Under native conditions, $(DNA–LLD)_2$ showed less electrophoresis mobility than F-dsDNA and $(DNA–TXN)_2$ (lanes i–iii, down Figures 5B and S16), while single-stranded oligo DNA-2LLD had the slowest migration rate (lane iv, down Figures 5B and S16). However, $(DNA–TXN)_2$ migrated faster than nonalkylated F-dsDNA (lanes i and ii, down Figures 5B and S16; lanes i and ii, Figures 5C and S16), with the anomalous relationship between the molecular weight and migration rate of $(DNA–TXN)_2$, further indicating that under native conditions, TXN interacts with DNA, making the structure more compact and causing the

https://doi.org/10.1021/jacsau.4c00611
JACS Au 2024, 4, 3641–3648

complex to pass through the gel matrix more easily, thus leading to an increase in the migration rate.

Hybridization experiments were next carried out between each alkylated single strand and F-ssDNA by mixing each component in the same proportions and annealing in solution. Native PAGE showed that the single-stranded DNA-TXN complex could hybridize with F-ssDNA (lane vi, down Figures 5B and S16, lanes i−iii, Figures 5C and S16); neither DNA−LLD nor DNA−2LLD could form a hybrid dsDNA with F-ssDNA (lanes vii and viii, Figures 5B and S16). DNA−2LLD always existed as a single chain that could not hybridize with any strand including DNA−LLD or itself (lanes viii and ix, Figures 5B and S16).

To further investigate the different biological effects of TXN and LLD, we conducted another alkylation assay using linearized plasmid pJL1 (2504 bp with 46% GC) with different ratios of drug to G equivalent, and Gelred was used to stain for a higher response to dsDNA than ssDNA. For LLD, even with only 0.5% G undergoing alkylation (1‰ total number of bases, alkylated 5 times on average based on gel results), the alkylated DNA migrated more slowly than nonalkylated, linearized plasmid (Figures 5D and S16). This indicated that LLD alkylated long-chain dsDNA in a mode identical to F-dsDNA, causing dsDNA destabilization, resulting in a loose helical structure. In comparison, at low concentrations of TXN (0.5% G equivalent), its alkylation on plasmid did not cause a significant variation in the migration rate of DNA, similar to that in TXN's reaction with F-dsDNA. When the concentration of TXN became higher (>5% G equivalent), the migration rate of alkylated DNA slowed down. The gel image underwent high contrast treatment, which showed that the color of linearized plasmids in the TXN group appeared obviously red; while in the LLD group, the color was weakened after adding a high equivalent of LLD, but green fluorescence from LLD appeared (Figure S16). These results indicated that the LLD-alkylated DNA double helix was more unstable than TX*N*-alkylated dsDNA, in line with the results from the T_m measurement (Figure 5A).

DISCUSSION

In this study, we determined solution structures of F-dsDNA, $(DNA{-}TXN)_2$, and $(DNA{-}LLD)_2$. The solution structure of $(DNA{-}TXN)_2$ had an rmsd value of 2.11 Å with the crystal structure 3C2J upon being superimposed. In the minor groove, the hydrogen bond between 2-OH of TXN and the O4′ atom in the sugar ring of base C_3 (C_{11}) in structure 3C2J was not observed in the solution structure (Figure S11), which may result in sugar S1 interacting more with solvents, making the interaction between sugar S1 and the minor groove of dsDNA in solution weaker than that in the crystal status. At the same time, in the solution structure of the $(DNA{-}TXN)_2$ complex, the alkylation-generated 14-OH of TXN had a distance of 3.1 Å with 3″−OH of sugar S2, smaller than that (3.4 Å) in the crystal structure, suggesting an intramolecular hydrogen bond between them in the solution state (Figure 4A). This conformational change resulted in sugar S2 far away from base A_1 (A_9). For $(DNA{-}LLD)_2$, the 4′-substituted sugars of TXN and LLD follow a similar binding mode with DNA, indicating that the sugar at the minor groove determines the molecule's binding form with DNA. The interaction between the $-NH_2$ of the G_6 base and sugar S1 and between the 2-OH of drugs and A_2 base together determine the drug insertion position (Figure 4B,C), while the substituents in the major groove caused the difference in DNA−drug complex stability. LLD has a larger substituent at the major groove and fewer interactions with DNA, which to a certain degree affect the helical structure of DNA (Figure 4A,D). Therefore, alkylation of dsDNA by LLD disrupts the stability of the DNA spatial structure. In addition, the orientation of the aromatic ring of the alkylated base G_6 (G_{14}) in the $(DNA{-}LLD)_2$ complex was also almost same as that in the $(DNA{-}TXN)_2$ complex but obviously different from that in the reported TXN covalently bound RET G4-DNA complex (pdb code 8GP7)[8] (Figure S14).

Through gel electrophoresis experiments, it was observed that under native conditions, LLD exhibited a slower migration rate, suggesting that the double-stranded complex is looser, resulting in a larger volume and making it more difficult to pass through the gel pores. Monoalkylation of dsDNA by LLD was more prone to destabilize the dsDNA conformation than TXN alkylation. Based on the results of hybridization experiments, it was concluded that DNA−LLD could not form a hybrid dsDNA with F-ssDNA and had a tendency to unwind. In contrast, TXN-alkylated ssDNA could hybridize with nonalkylated ssDNA and itself. From the prior results, we can infer the following reaction process (Figure 5E): TXN alkylation on dsDNA could maintain its double-stranded conformation during the entire process. In contrast, after one strand of dsDNA was alkylated by LLD, this LLD-alkylated dsDNA undergoes strand separation, forming F-ssDNA and single-strand DNA−LLD. DNA−LLD could reform into a double-strand DNA with itself or further be alkylated by LLD on base G_5 (G_{13}) and generated DNA−2LLD. Previous research has shown that in B-form DNA, the G base adjacent to the T base at the 5′ position is more easily recognized and alkylated by this type of molecule.[9] Therefore, we believe that the monoalkylation of G_5 (G_{13}) occurs on ssDNA rather than dsDNA, which was in line with the result that LLD cannot further alkylate $(DNA{-}LLD)_2$ Figure 2A, line (iii). During LLD alkylation, dsDNA unwound and generated ssDNA after F-dsDNA had been alkylated by one molecule of LLD, which also explains why the yield of DNA-LLD* is much more than that of DNA-TXN*(Figure 2A, lines ii and vi).

LLD was first isolated in 1989, later than TXN in 1981,[6,20] and in vitro experiment showed its lower bioactivities than that of TXN.[11,17,19] However, LLD was the first molecule of this family to enter clinical research.[7] In preclinical animal experiments on certain tumors, LLD had shown a higher median survival time.[6,20] TXN and LLD covalently bind to the 3′ end of guanines, unlike alkylating agents such as hedamycin, which covalently bind to the 5′ end of guanine. Both TXN and LLD underwent similar chemical reactions with DNA, involving nucleophilic ring opening of the epoxide and the formation of a covalent bond between C17 and N7 of guanine, which can damage DNA through changes in chemical bonds. In addition, LLD can also seriously reduce the stability of the double strand after binding, destroying the integrity of the dsDNA. This "dual mechanism" may be the reason why LLD has better animal experiments activity.

Phase I clinical trials of LLD mentioned its cardiac toxicity, which is also the main side effect of many other anthracyclines' anticancer drugs. However, the differences in sugar substitutions often led to variations in ultimate toxic side effects. For example, doxorubicin and epirubicin have similar anticancer mechanisms, due to differences in sugar substitution groups, epirubicin exhibits lighter cardiac toxicity.[26] LLD and TXN also have identical skeletal structures and similar mechanisms of biological activity, and this study provides ideas for further modification of

https://doi.org/10.1021/jacsau.4c00611
JACS Au 2024, 4, 3641−3648

this class of molecules, suggesting that retaining the substitution at the 4 position of the sugar S1 can keep the high biological reactivity of these molecules, altering the form of the substitution group at the major groove, such as the number of sugar groups and their positions, and may obtain new antibodies that not only exhibits good antitumor activity but also shows a lower side effect.

In previous studies, through chemical synthesis and combinatorial biosynthesis methods, many molecules with the same backbones and spiro epoxide rings as TXN or LLD have been obtained,[10−17] including some derivatives with the active moiety on the sugar group that can be modified (such as diazo group[11]). In this work, by analyzing the NMR structures of DNA−drug complexes in aqueous solutions, we found that TXN and LLD have fewer hydrogen bond interactions with DNA in the major groove. By keeping the 4-position glycosyl substituent unchanged, variations of the substituent groups located at the major groove will have little influence on DNA compound identification. The modifications of the sugars for major groove binding may not seriously affect the bioactivity seriously. This finding may provide a useful clue to guide the next modifications in drug development. Additionally, given the nanomolar-level biological activity, these molecules may exhibit the potential to be payloads for ADC drugs in the near future.

In summary, it was elucidated that TXN alkylation of DNA could maintain the dsDNA conformation even when it was alkylated by an extremely large amount of TXN. In contrast, LLD alkylation of DNA was prone to cause dsDNA to be much more unstable. Sufficient alkylation of dsDNA by LLD could induce significant dsDNA helix deformation, resulting in dsDNA unwinding. These findings may provide a deep interpretation of why LLD performed better than TXN in in vivo preclinical trials, which originated from the different DNA bindings caused by different sugar substitutions.

■ ASSOCIATED CONTENT

Supporting Information

The Supporting Information is available free of charge at https://pubs.acs.org/doi/10.1021/jacsau.4c00611.

F-dsDNA preparation and its alkylation by TXN or LLD, characterization of the complexes $(DNA-TXN)_2$, DNA−LLD*, $(DNA-LLD)_2$, and DNA−2LLD by HPLC, native and denaturing electrophoresis of DNA, UV−vis spectra, DSC and 1D ^{1}H NMR spectra; chemical shift perturbation, the whole process of NMR signal assignment, solution structural determination and analysis of free F-dsDNA, and of its covalent complexes $(DNA-TXN)_2$ and $(DNA-LLD)_2$, extended alkylation of linearized plasmid pJL1 by TXN and LLD; the final chemical shift tables of the protons of free F-dsDNA and its complexes $(DNA-TXN)_2$ and $(DNA-LLD)_2$, NOE assignment in the complex $(DNA-LLD)_2$, and in the complex $(DNA-TXN)_2$ (PDF)

Accession Codes

The atomic coordinates of free F-dsDNA, TXN, and LLD covalently bound F-dsDNA had been deposited in the Protein Data Bank (http://wwpdb.org/) with codes 8Y1I, 8XIC, and 8XC7, respectively; the corresponding chemical shift assignment for them had been deposited in the Biological Magnetic Resonance Data Bank (BMRB) under accession codes 36641, 36627, and 36621, respectively.

■ AUTHOR INFORMATION

Corresponding Authors

Chunyang Cao − *State Key Laboratory of Chemical Biology, Shanghai Institute of Organic Chemistry, University of Chinese Academy of Sciences, Chinese Academy of Sciences, Shanghai 200032, China;* orcid.org/0000-0001-7865-8249; Email: ccao@sioc.ac.cn

Gong-Li Tang − *State Key Laboratory of Chemical Biology, Shanghai Institute of Organic Chemistry, University of Chinese Academy of Sciences, Chinese Academy of Sciences, Shanghai 200032, China; School of Chemistry and Materials Science, Hangzhou Institute for Advanced Study, University of Chinese Academy of Sciences, Hangzhou, Zhejiang 310024, China;* orcid.org/0000-0003-3149-4683; Email: gltang@sioc.ac.cn

Authors

Ruo-Qin Gao − *State Key Laboratory of Chemical Biology, Shanghai Institute of Organic Chemistry, University of Chinese Academy of Sciences, Chinese Academy of Sciences, Shanghai 200032, China*

Xiao-Dong Hu − *State Key Laboratory of Chemical Biology, Shanghai Institute of Organic Chemistry, University of Chinese Academy of Sciences, Chinese Academy of Sciences, Shanghai 200032, China*

Qiang Zhou − *State Key Laboratory of Chemical Biology, Shanghai Institute of Organic Chemistry, University of Chinese Academy of Sciences, Chinese Academy of Sciences, Shanghai 200032, China*

Xian-Feng Hou − *State Key Laboratory of Chemical Biology, Shanghai Institute of Organic Chemistry, University of Chinese Academy of Sciences, Chinese Academy of Sciences, Shanghai 200032, China*

Complete contact information is available at: https://pubs.acs.org/10.1021/jacsau.4c00611

Author Contributions

Gong-Li Tang, Chunyang Cao, and Ruo-Qin Gao designed research; Ruo-Qin Gao, Qiang Zhou, and Xian-Feng Hou performed research; Ruo-Qin Gao, Xiao-Dong Hu, Chunyang Cao, and Gong-Li Tang analyzed data; and Ruo-Qin Gao, Chunyang Cao, and Gong-Li Tang wrote the paper. CRediT: **Chunyang Cao** conceptualization, formal analysis, project administration, supervision, writing - original draft, writing - review & editing; **Gong-Li Tang** conceptualization, formal analysis, funding acquisition, project administration, supervision.

Notes

The authors declare no competing financial interest.

■ ACKNOWLEDGMENTS

This work was supported by grants from the National Natural Science Foundation of China (22137009, 22077134, 22177127, and 22174155). The authors also thank all facility team members of NMR Facilities, National Center of Protein Sciences Shanghai, and Steady High Magnetic Field Facilities, High-Field Magnetic Laboratory, CAS, Hefei, and the NMR center of Shanghai Institute of Materia Medica, CAS, China for their help with NMR spectra acquirement.

REFERENCES

(1) Gewirtz, D. A. A critical evaluation of the mechanisms of action proposed for the antitumor effects of the anthracycline antibiotics Adriamycin and daunorubicin. *Biochem. Pharmacol.* **1999**, *57* (7), 727−741.

(2) Wu, J. G.; Ling, X.; Pan, D. L.; Apontes, P.; Song, L.; Liang, P.; Altieri, D. C.; Beerman, T.; Li, F. Z. Molecular mechanism of inhibition of survivin transcription by the GC-rich sequence-selective DNA binding antitumor agent, hedamycin - Evidence of survivin down-regulation associated with drug sensitivity. *J. Biol. Chem.* **2005**, *280* (10), 9745−9751.

(3) Fitzner, A.; Frauendorf, H.; Laatsch, H.; Diederichsen, U. Formation of gutingimycin: analytical investigation of trioxacarcin A-mediated alkylation of dsDNA. *Anal. Bioanal. Chem.* **2008**, *390* (4), 1139−1147.

(4) Pröpper, K.; Dittrich, B.; Smaltz, D. J.; Magauer, T.; Myers, A. G. Crystalline guanine adducts of natural and synthetic trioxacarcins suggest a common biological mechanism and reveal a basis for the instability of trioxacarcin A. *Bioorg. Med. Chem. Lett.* **2014**, *24* (18), 4410−4413.

(5) Chen, X. R.; Bradley, N. P.; Lu, W.; Wahl, K. L.; Zhang, M.; Yuan, H.; Hou, X. F.; Eichman, B. F.; Tang, G. L. Base excision repair system targeting DNA adducts of trioxacarcin/LL-D49194 antibiotics for self-resistance. *Nucleic Acids Res.* **2022**, *50* (5), 2417−2430.

(6) Maiese, W. M.; Labeda, D. P.; Korshalla, J.; Kuck, N.; Fantini, A. A.; Wildey, M. J.; Thomas, J.; Greenstein, M. LL-D49194 antibiotics, a novel family of antitumor agents. Taxonomy, fermentation and biological properties. *J. Antibiot.* **1990**, *43* (3), 253−258.

(7) Cassidy, J.; Graham, M. A.; Huinink, W. T. B.; McDaniel, C.; Setanoians, A.; Rankin, E. M.; Kerr, D. J.; Kaye, S. B. Phase I clinical study of LL-D49194 alpha 1 with retrospective pharmacokinetic investigations in mice and humans. The EORTC ECTG. *Cancer Chemother. Pharmacol.* **1993**, *31* (5), 395−400.

(8) Yin, S. W.; Lan, W. X.; Hou, X. F.; Liu, Z. J.; Xue, H. J.; Wang, C. X.; Tang, G. L.; Cao, C. Y. Trioxacarcin A Interactions with G-Quadruplex DNA Reveal Its Potential New Targets as an Anticancer Agent. *J. Med. Chem.* **2023**, *66* (10), 6798−6810.

(9) Pfoh, R.; Laatsch, H.; Sheldrick, G. M. Crystal structure of trioxacarcin A covalently bound to DNA. *Nucleic Acids Res.* **2008**, *36* (10), 3508−3514.

(10) Svenda, J.; Hill, N.; Myers, A. G. A multiply convergent platform for the synthesis of trioxacarcins. *Proc. Natl. Acad. Sci. U.S.A.* **2011**, *108* (17), 6709−6714.

(11) Magauer, T.; Smaltz, D. J.; Myers, A. G. Component-based syntheses of trioxacarcin A, DC-45-A1 and structural analogues. *Nat. Chem.* **2013**, *5* (10), 886−893.

(12) Qi, L. H.; Zhang, M.; Pan, H. X.; Chen, X. D.; Tang, G. L. Production of a trioxacarcin analogue by engineering of its biosynthetic pathway. *Chin. J. Org. Chem.* **2014**, *34* (7), 1376−1381.

(13) Nicolaou, K. C.; Cai, Q.; Qin, B.; Petersen, M. T.; Mikkelsen, R. J. T.; Heretsch, P. Total synthesis of trioxacarcin DC-45-A2. *Angew. Chem., Int. Ed.* **2015**, *54* (10), 3074−3078.

(14) Zhang, M.; Hou, X. F.; Qi, L. H.; Yin, Y.; Li, Q.; Pan, H. X.; Chen, X. Y.; Tang, G. L. Biosynthesis of trioxacarcin revealing a different starter unit and complex tailoring steps for type II polyketide synthase. *Chem. Sci.* **2015**, *6* (6), 3440−3447.

(15) Nicolaou, K. C.; Cai, Q.; Sun, H. B.; Qin, B.; Zhu, S. G. Total synthesis of trioxacarcins DC-45-A1, A, D, C, and C7″-epi-C and full structural assignment of trioxacarcin C. *J. Am. Chem. Soc.* **2016**, *138* (9), 3118−3124.

(16) Nicolaou, K. C.; Chen, P. X.; Zhu, S. G.; Cai, Q.; Erande, R. D.; Li, R. F.; Sun, H. B.; Pulukuri, K. K.; Rigol, S.; Aujay, M.; Sandoval, J.; Gavrilyuk, J. Streamlined total synthesis of trioxacarcins and its application to the design, synthesis, and biological evaluation of analogues thereof. discovery of simpler designed and potent trioxacarcin analogues. *J. Am. Chem. Soc.* **2017**, *139* (43), 15467−15478.

(17) Dong, L.; Shen, Y.; Hou, X. F.; Li, W. J.; Tang, G. L. Discovery of druggability-improved analogues by investigation of the LL-D49194α1 biosynthetic pathway. *Org. Lett.* **2019**, *21* (7), 2322−2325.

(18) Shen, Y.; Nie, Q. Y.; Yin, Y.; Pan, H. X.; Xu, B.; Tang, G. L. Production of a trioxacarcin analog by introducing a C-3 dehydratase into deoxysugar biosynthesis. *Acta Biochim. Biophys. Sin.* **2019**, *51* (5), 539−541.

(19) Maskey, R. P.; Helmke, E.; Kayser, O.; Fiebig, H. H.; Maier, A.; Busche, A.; Laatsch, H. Anti-cancer and antibacterial trioxacarcins with high anti-malaria activity from a marine Streptomycete and their absolute stereochemistry. *J. Antibiot.* **2004**, *57* (12), 771−779.

(20) Tomita, F.; Tamaoki, T.; Morimoto, M.; Fujimoto, K. Trioxacarcins, novel antitumor antibiotics. I. Producing organism, fermentation and biological activities. *J. Antibiot.* **1981**, *34* (12), 1519−1524.

(21) Yang, K.; Qi, L. H.; Zhang, M.; Hou, X. F.; Pan, H. X.; Tang, G. L.; Wang, W.; Yuan, H. The SARP family regulator Txn9 and two-component response regulator Txn11 are key activators for trioxacarcin biosynthesis in Streptomyces bottropensis. *Curr. Microbiol.* **2015**, *71* (4), 458−464.

(22) Yin, Y.; Shen, Y.; Meng, S.; Zhang, M.; Pan, H. X.; Tang, G. L. Characterization of a membrane-bound *o*-acetyltransferase involved in trioxacarcin biosynthesis offers insights into its catalytic mechanism. *Chin. J. Chem.* **2020**, *38* (12), 1607−1611.

(23) Hou, X. F.; Song, Y. J.; Zhang, M.; Lan, W. X.; Meng, S.; Wang, C. X.; Pan, H. X.; Cao, C. Y.; Tang, G. L. Enzymology of anthraquinone-γ-pyrone ring formation in complex aromatic polyketide biosynthesis. *Angew. Chem., Int. Ed.* **2018**, *57* (41), 13475−13479.

(24) Kou, Y.; Koag, M. C.; Lee, S. Structural and kinetic studies of the effect of guanine N7 alkylation and metal cofactors on DNA replication. *Biochemistry* **2018**, *57* (34), 5105−5116.

(25) Garabet, A.; Liu, L. T.; Chalikian, T. V. Heat capacity changes associated with G-quadruplex unfolding. *J. Chem. Phys.* **2023**, *159* (5), 055101.

(26) Launchbury, A. P.; Habboubi, N. Epirubicin and doxorubicin - a comparison of their characteristics, therapeutic activity and toxicity. *Cancer Treat. Rev.* **1993**, *19* (3), 197−228.

https://doi.org/10.1021/jacsau.4c00611
JACS Au 2024, 4, 3641−3648